Electronic Supplementary Material (ESI) for Nanoscale.

Supporting Information

Polyoxometalate Precursors for Precisely Controlling Synthesis of Bimetallic Sulfide Heterostructure through Nucleation-Doping Competition

Yu-Jia Tang,[a] A-Man Zhang,[a] Hong-Jing Zhu,[a] Long-Zhang Dong,[a] Xiao-Li Wang,[a] Shun-Li Li,[a] Min Han,[a] Xiang-Xin Xu[a] and Ya-Qian Lan*[a]

[a] Jiangsu Collaborative Innovation Centre of Biomedical Functional Materials, Jiangsu Key Laboratory of New Power Batteries, School of Chemistry and Materials Science, Nanjing Normal University, Nanjing 210023, China

Chemicals and Materials

Sodium molybdate dihydrate ($Na_2MoO_4{\cdot}2H_2O$, AR), cobalt sulfate heptahydrate ($CoSO_4{\cdot}7H_2O$, AR), ammonium heptamolybdate tetrahydrate ($(NH_4)_6Mo_7O_{24}{\cdot}4H_2O$, AR), ferric sulfate hexahydrate ($Fe_2(SO_4)_3{\cdot}6H_2O$, AR) and hydrogen peroxide (H_2O_2, 30%, AR) were purchased from Sinopharm Chemical Reagent Co., Ltd. Nickle sulfate hexahydrate ($NiSO_4{\cdot}6H_2O$, AR) was bought from Aladdin Reagent. Thiourea (CH_4N_2S, AR) was purchased from Shanghai Lingfeng Chemical Reagent Co., Ltd. 20% Pt/C, IrO_2 and Nafion solution (5 wt%) were bought from Sigma-Aldrich. Carbon Cloth (W0S1002) was purchased from CeTech Co., Ltd.

Synthesis of Anderson-type POMs

*$(NH_4)_4[Co(II)Mo_6O_{24}H_6]{\cdot}6H_2O$ (**$CoMo_6$**):* $CoSO_4{\cdot}7H_2O$ (4.2 g, 15 mmol) and H_2O_2 (2 g, 30 %) in 30 mL H_2O were added into a boiling aqueous solution of $(NH_4)_6Mo_7O_{24}{\cdot}4H_2O$ (30.9 g, 25 mmol) in 260 mL H_2O. The obtained solution was further evaporated on a steam-bath for a certain time and cooled to room temperature to get the green crystals of $CoMo_6$. The products were collected by filtration and dried at 60 °C overnight.

*$(NH_4)_4[Ni(II)Mo_6O_{24}H_6]{\cdot}5H_2O$ (**$NiMo_6$**):* $NiSO_4{\cdot}6H_2O$ (0.78 g, 3 mmol) in 20 mL H_2O was added into a boiling aqueous solution of $(NH_4)_6Mo_7O_{24}{\cdot}4H_2O$ (5.2 g, 4.2 mmol) in 80 mL H_2O. The obtained solution was further evaporated on a steam-bath and cooled to room temperature to get the light blue crystals of $NiMo_6$. $NiMo_6$ compounds were recrystallized twice from water to obtain pure crystals.

*$(NH_4)_3[Fe(III)Mo_6O_{24}H_6]{\cdot}6H_2O$ (**$FeMo_6$**):* $Fe_2(SO_4)_3{\cdot}6H_2O$ (1.2 g, 3.1 mmol) in 20 mL H_2O was added into a boiling aqueous solution of $(NH_4)_6Mo_7O_{24}{\cdot}4H_2O$ (5.2 g, 4.2 mmol) in 80 mL H_2O. The obtained solution was further evaporated on a steam-bath and cooled to room temperature to get the yellow crystals of $FeMo_6$. The products were collected by filtration and dried at 60 °C overnight.

X-ray crystallography

The single-crystal diffraction data for $CoMo_6$ was collected on Bruker AXS Apex II CCD diffractometer at 298 K. The X-ray generator was operated at 50 kV and 30 mA using Mo-Kα (λ = 0.71073 Å) radiation. The crystal structures were solved and refined by full matrix least-squares methods against F^2 using the SHELXL-2014 program package and Olex-2 software. All non-hydrogen atoms were refined with anisotropic displacement parameters and hydrogen positions were fixed at calculated positions and refined isotropically. The crystallographic data and structure refinement for $CoMo_6$ are summarized in **Table S1**. CCDC 1561298 contain the supplementary crystallographic data for this paper. These data can be obtained free of charge from The Cambridge Crystallographic Data Centre.

The crystal structure of Anderson-type POMs ($CoMo_6$) was shown in **Figure S1**. $NiMo_6$ and $FeMo_6$ POMs have the same structures except for the central metal of Co replaced by Ni and Fe, respectively. The successful synthesis of three POMs were confirmed by FT-IR and PXRD characterizations (**Figure S2**). $CoMo_6$, $NiMo_6$ and

$FeMo_6$ show the similar characteristic peaks in the 950-850 cm^{-1} and 650-550 cm^{-1} regions because of the same Anderson molydopolyanions structures. PXRD spectra of as-prepared POMs all match well with the simulated patterns.

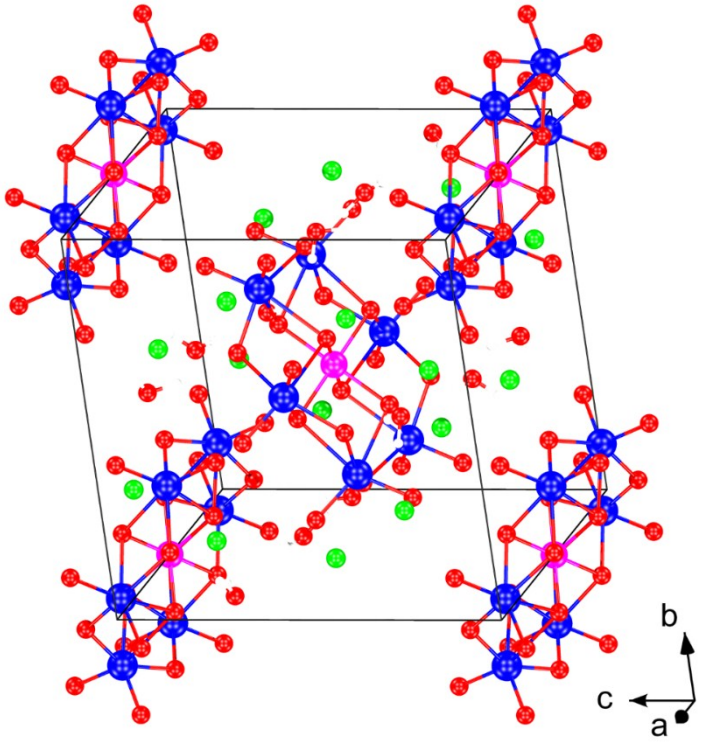

Figure S1. Crystal structure of $CoMo_6$ POMs. The blue, pink, red and green represent Mo, Co, O and N, respectively.

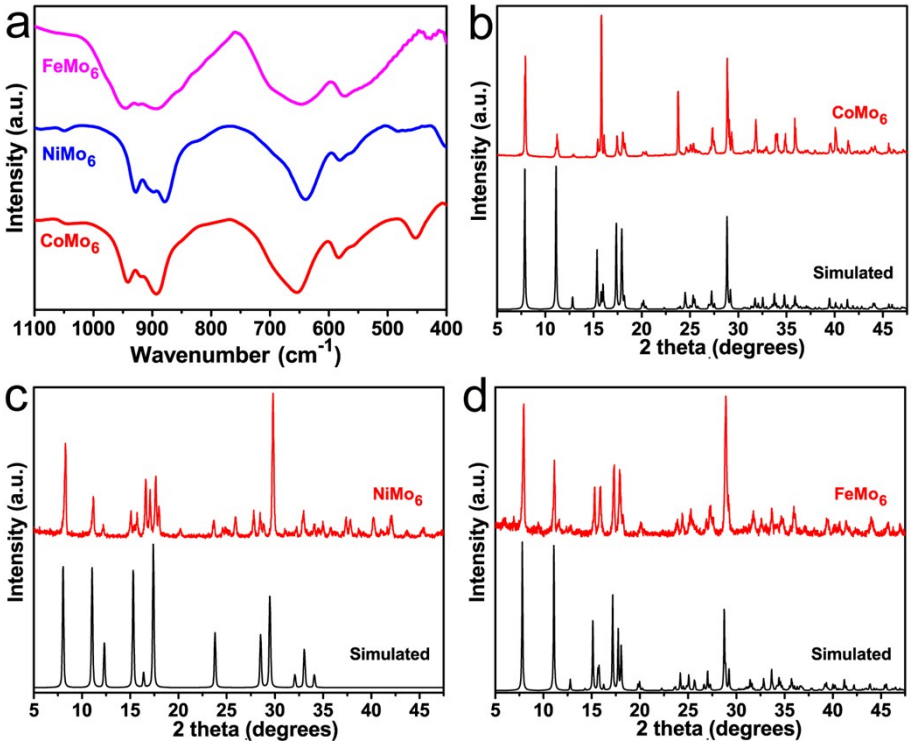

Figure S2. (a) FT-TR spectrum and (c-d) PXRD patterns of three Anderson-type POMs used in this work.

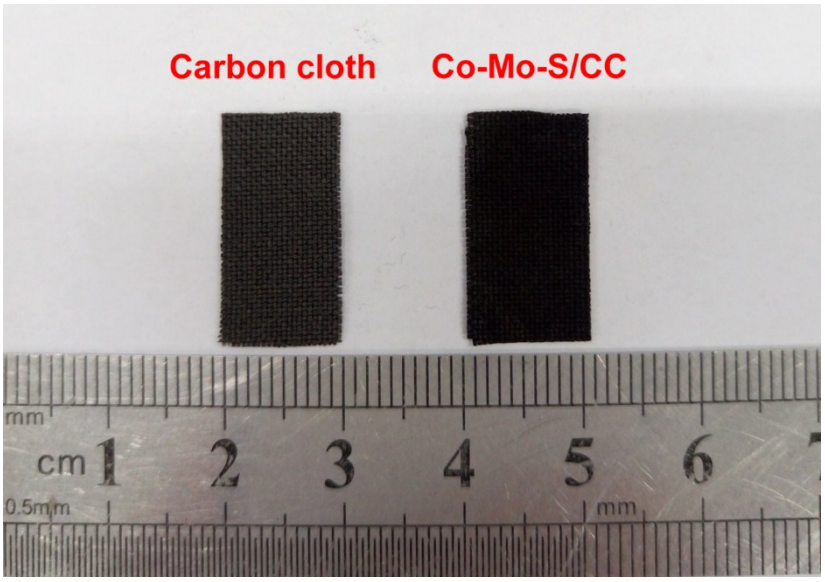

Figure S3. Optical images of pristine carbon cloth (left) and Co-Mo-S/CC electrode (right).

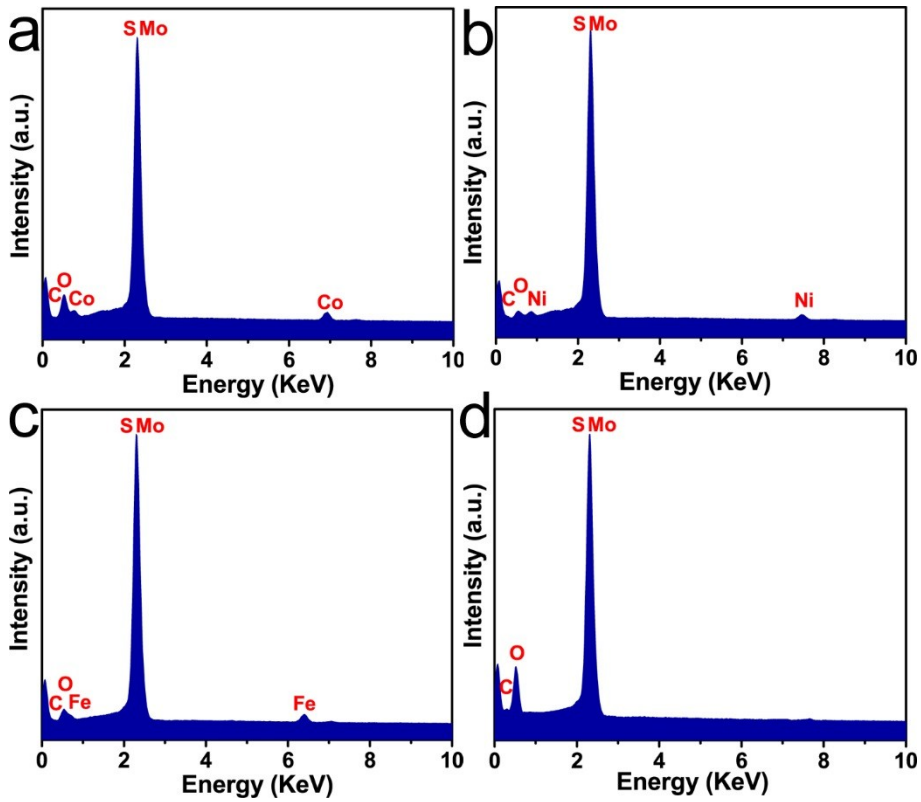

Figure S4. EDS spectra of (a) Co-Mo-S/CC, (b) Ni-Mo-S/CC, (c) Fe-Mo-S/CC and (d) MoS_2/CC.

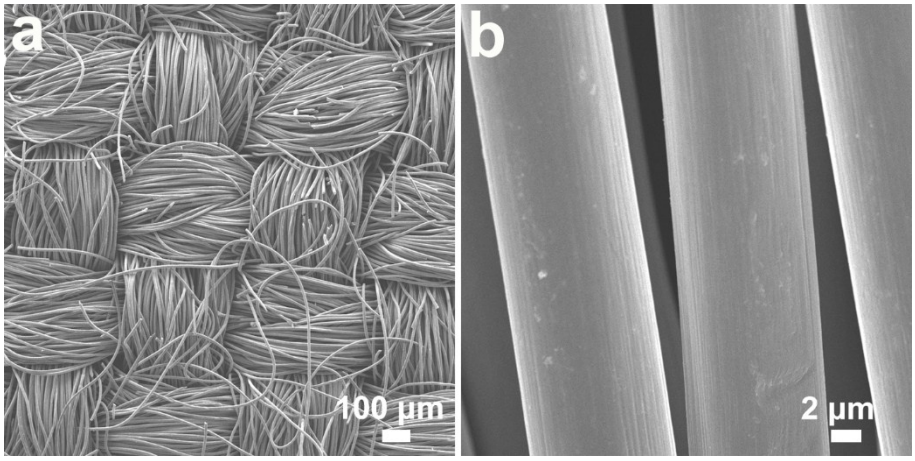

Figure S5. SEM image of pure carbon cloth (CC) at different scale.

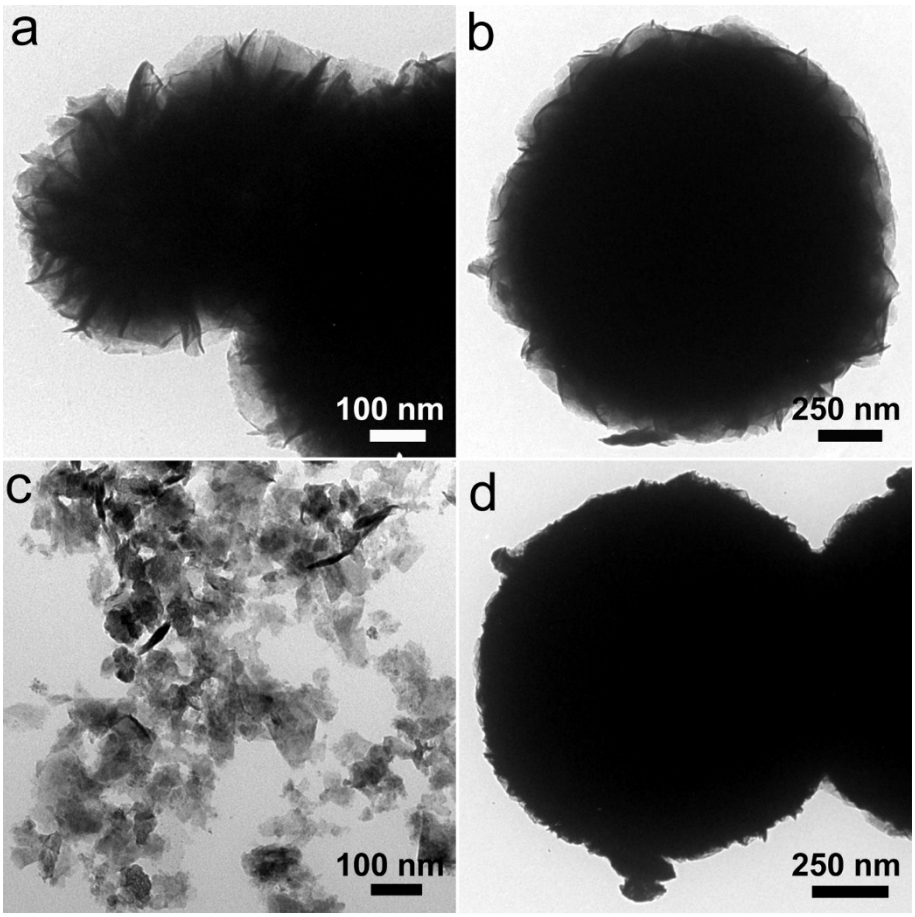

Figure S6. TEM images of (a) Co-Mo-S, (b) Ni-Mo-S, (c) Fe-Mo-S and (d) MoS_2.

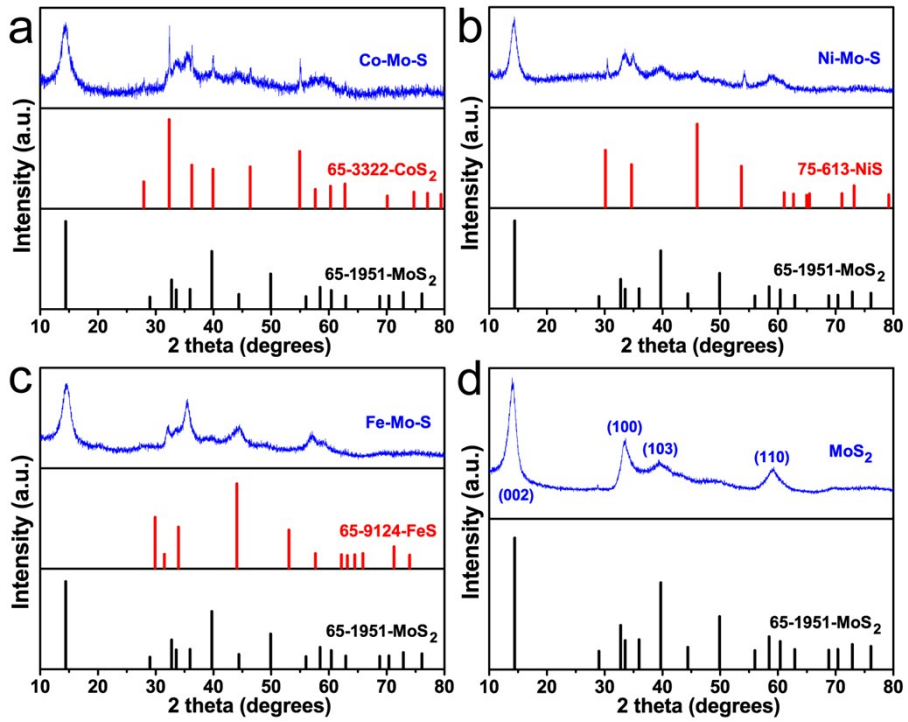

Figure S7. PXRD patterns of (a) Co-Mo-S, (b) Ni-Mo-S, (c) Fe-Mo-S and (d) MoS_2.

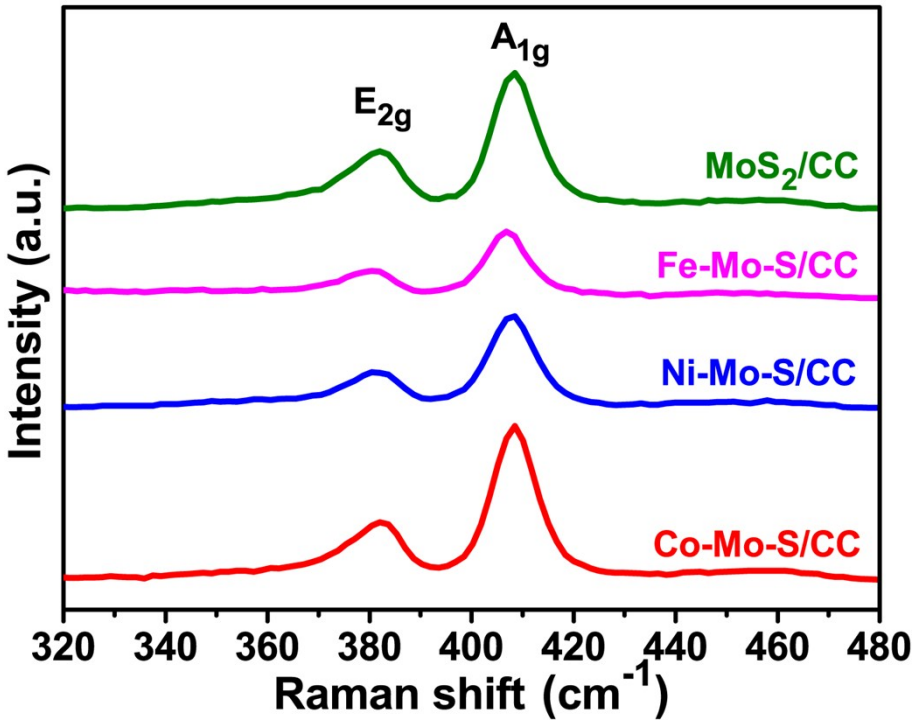

Figure S8. Raman spectrum of Co-Mo-S/CC, Ni-Mo-S/CC, Fe-Mo-S/CC and MoS_2/CC.

Raman spectrum displays the in-plane E_{2g} (382 cm^{-1}) and out-of-plane A_{1g} peaks (408 cm^{-1}), which is accord with the 2H-MoS_2. There are no peak shift and no other extra peaks, confirming that introducing the secondary metal does not destroy the pristine MoS_2 structures.

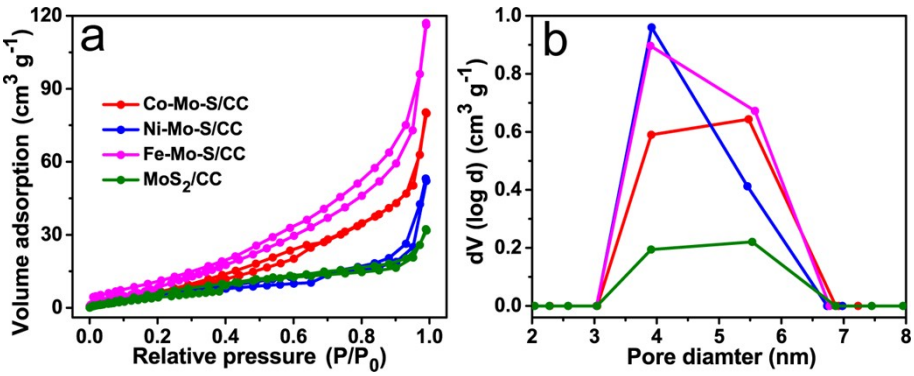

Figure S9. (a) N_2 adsorption-desorption isotherm of Co-Mo-S/CC, Ni-Mo-S/CC, Fe-Mo-S/CC and MoS_2/CC. (b) The pore size distribution analyzed by BJH method.

The specific surface area of Co-Mo-S/CC, Ni-Mo-S/CC, Fe-Mo-S/CC and MoS_2/CC samples is 32.7, 19.3, 68.3 and 18.6 m^2 g^{-1}, respectively. It is worth noting that Fe-Mo-S/CC has the largest surface area due to the growth of Fe-Mo-S nanosheets on CC directly without stacking into spheres. Co-Mo-S/CC has the second higher surface area because Co-Mo-S nanospheres can grow on CC evenly and densely, which is consistent with SEM image. The pore size distribution analysis exhibits that all samples have the mesopores with an average pore size of 3-6.5 nm.

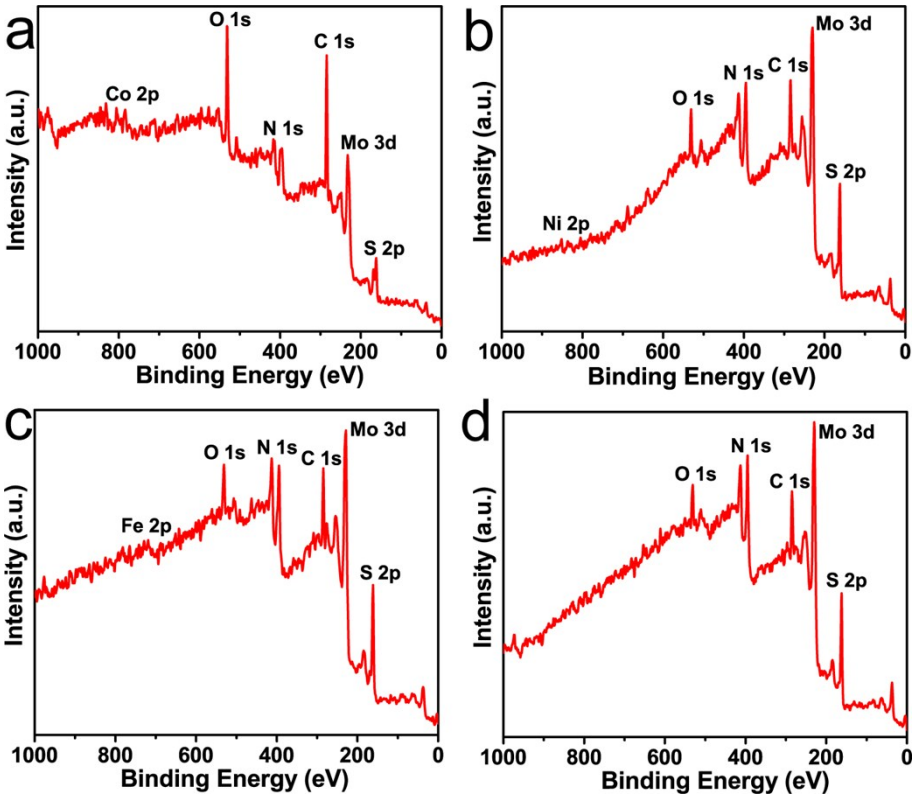

Figure S10. XPS spectra (a) Co-Mo-S/CC, (b) Ni-Mo-S/CC, (c) Fe-Mo-S/CC and (d) MoS_2/CC.

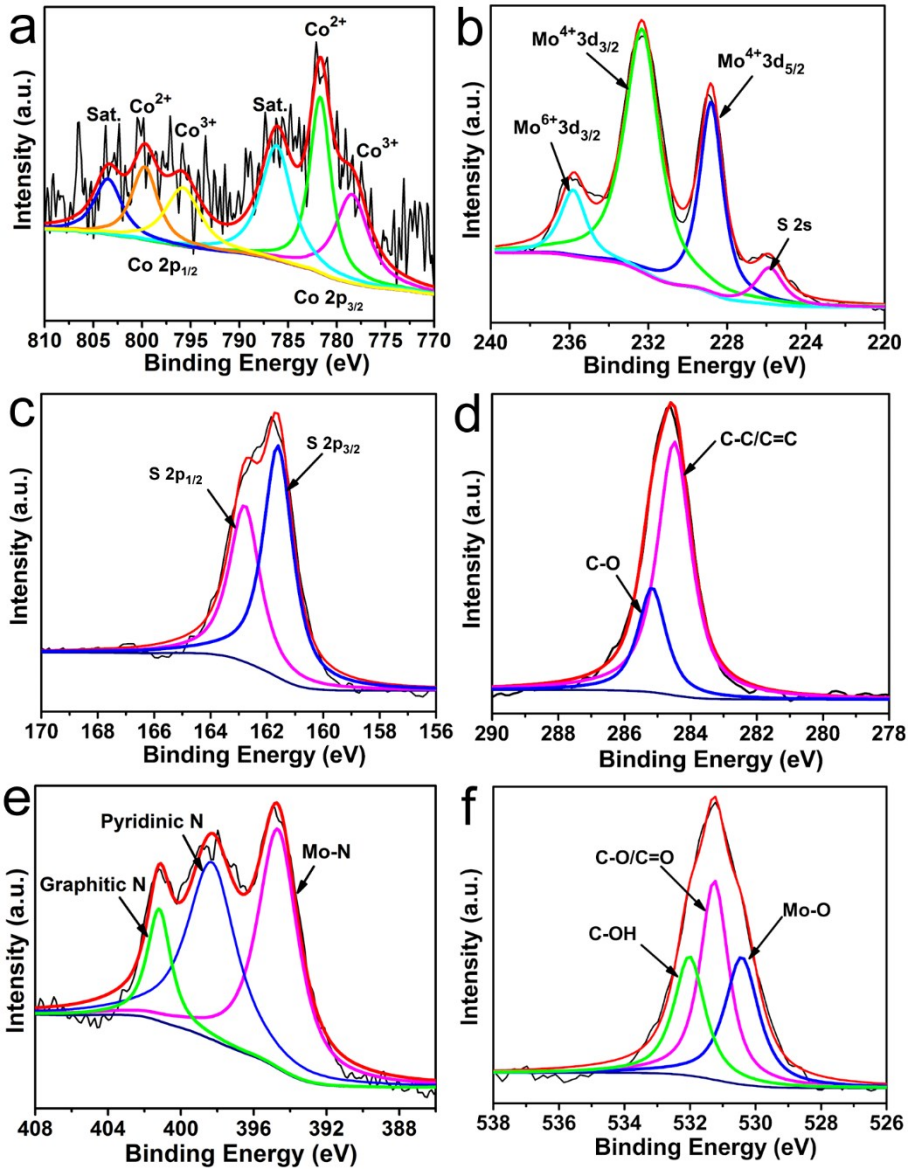

Figure S11. High resolution XPS spectra of (a) Co 2p, (b) Mo 3d, (c) S 2p, (d) C 1s, (e) N 1s and (f) O 1s for Co-Mo-S/CC sample.

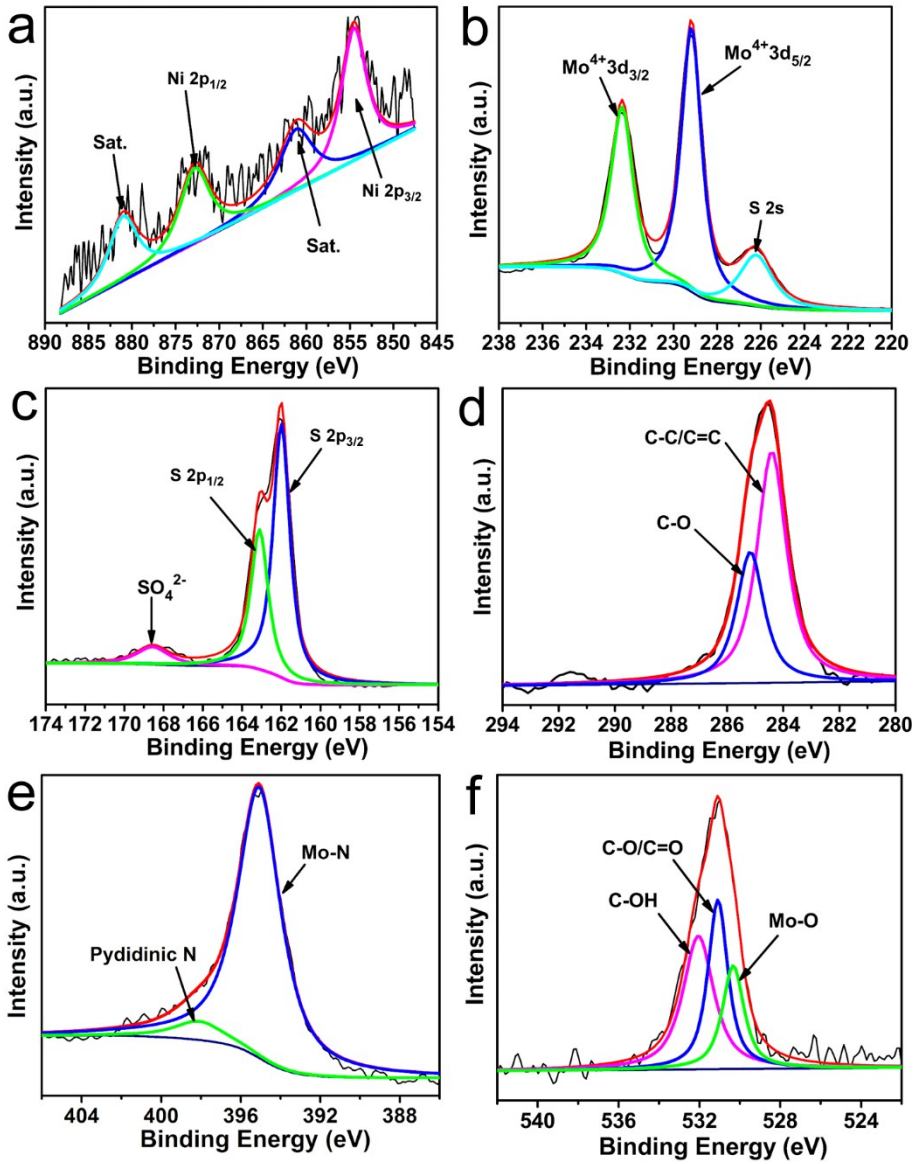

Figure S12. High resolution XPS spectra of (a) Ni 2p, (b) Mo 3d, (c) S 2p, (d) C 1s, (e) N 1s and (f) O 1s for Ni-Mo-S/CC sample.

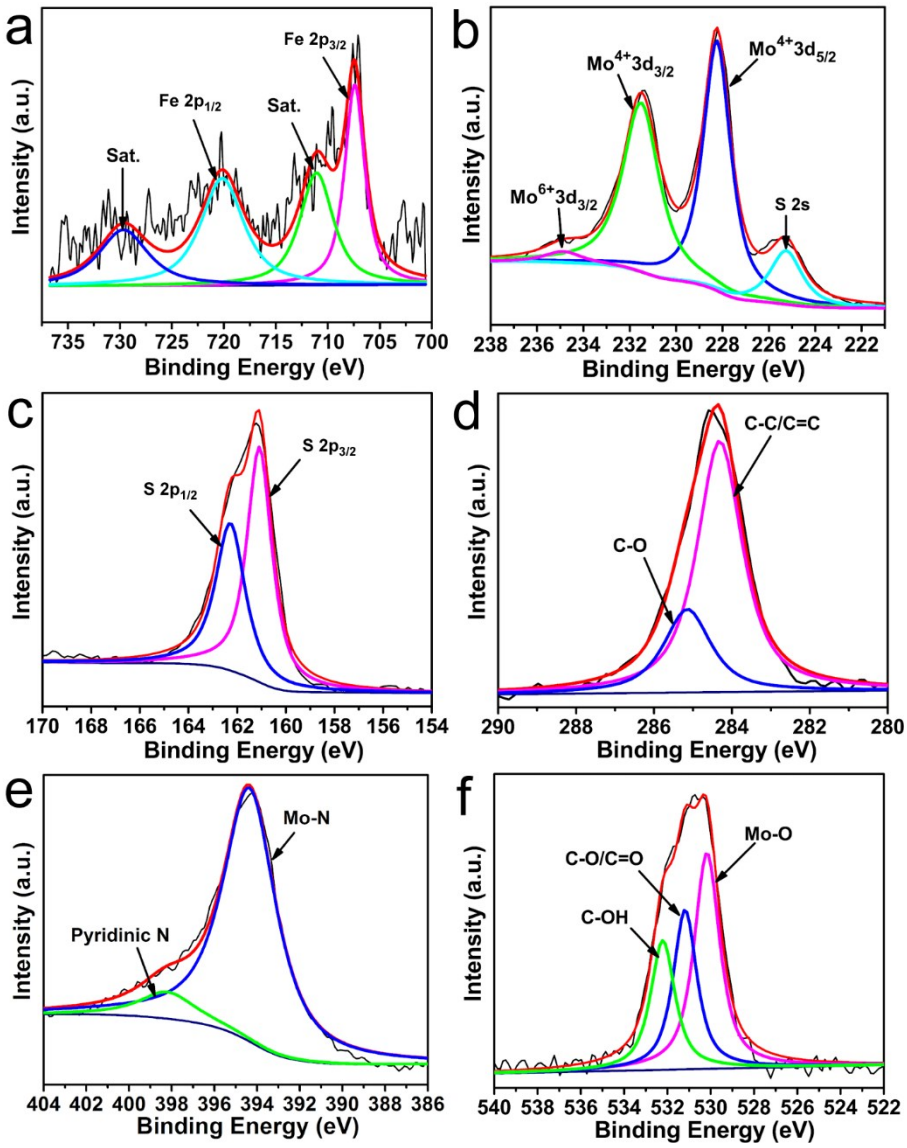

Figure S13. High resolution XPS spectra of (a) Fe 2p, (b) Mo 3d, (c) S 2p, (d) C 1s, (e) N 1s and (f) O 1s for Fe-Mo-S/CC sample.

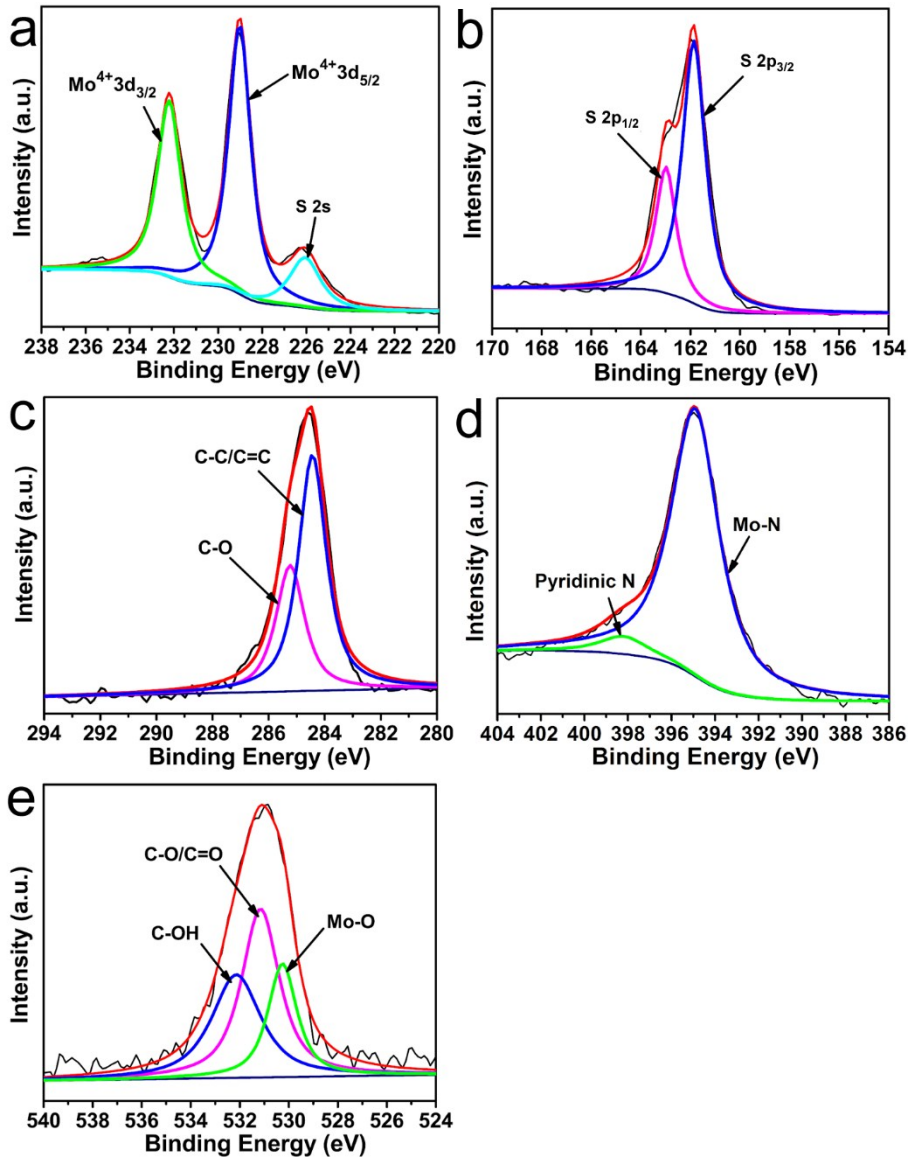

Figure S14. High resolution XPS spectra of (a) Mo 3d, (b) S 2p, (c) C 1s, (d) N 1s and (e) O 1s for MoS_2/CC sample.

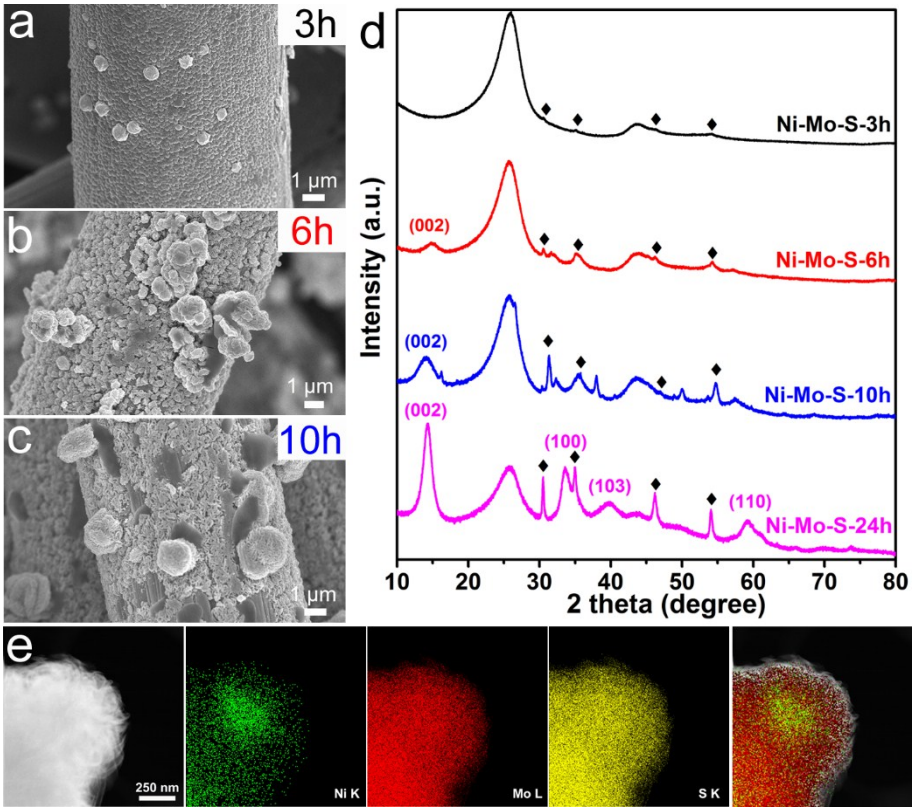

Figure S15. (a-c) SEM images of Ni-Mo-S/CC-t (t = 3 h, 6 h and10 h) obtained at different hydrothermal time. (d) PXRD spectra of Ni-Mo-S/CC-t obtained at different hydrothermal time (♦ represents the peaks of NiS). (e) EDS elemental mappings of Ni-Mo-S and overlay image of Ni, Mo and S elements. Ni is shown in green, Mo is shown in red and S is shown in yellow.

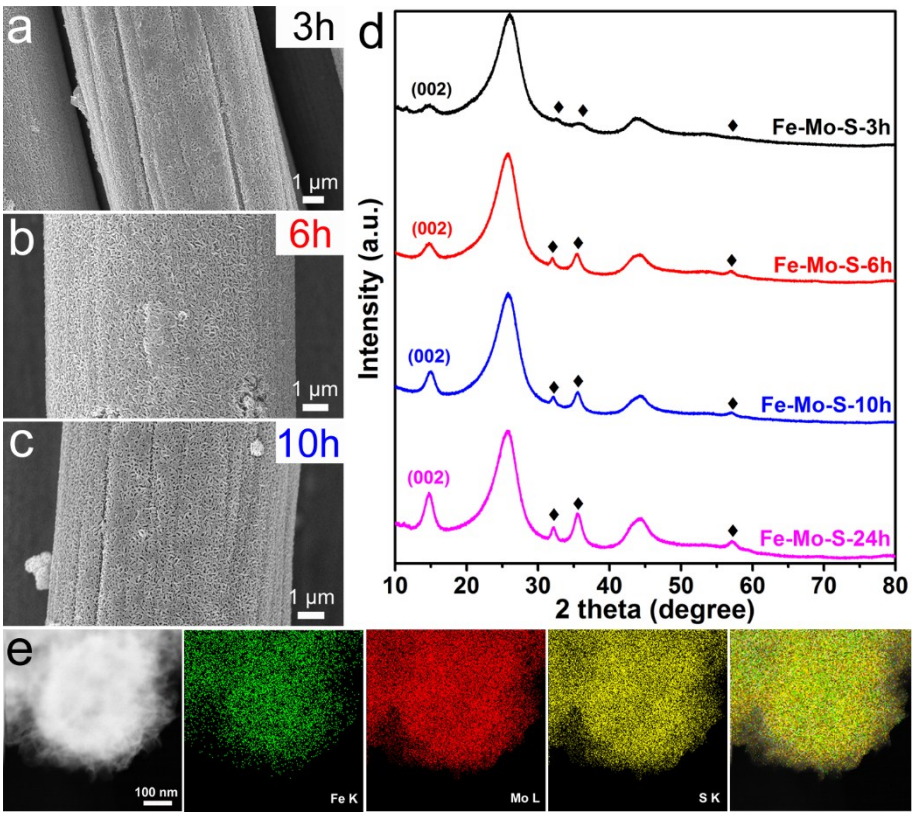

Figure S16. (a-c) SEM images of Fe-Mo-S/CC-t (t = 3 h, 6 h and 10 h) obtained at different hydrothermal time. (d) PXRD spectra of Fe-Mo-S/CC-t obtained at different hydrothermal time (♦ represents the peaks of FeS). (e) EDS elemental mappings of Fe-Mo-S and overlay image of Fe, Mo and S elements. Fe is shown in green, Mo is shown in red and S is shown in yellow.

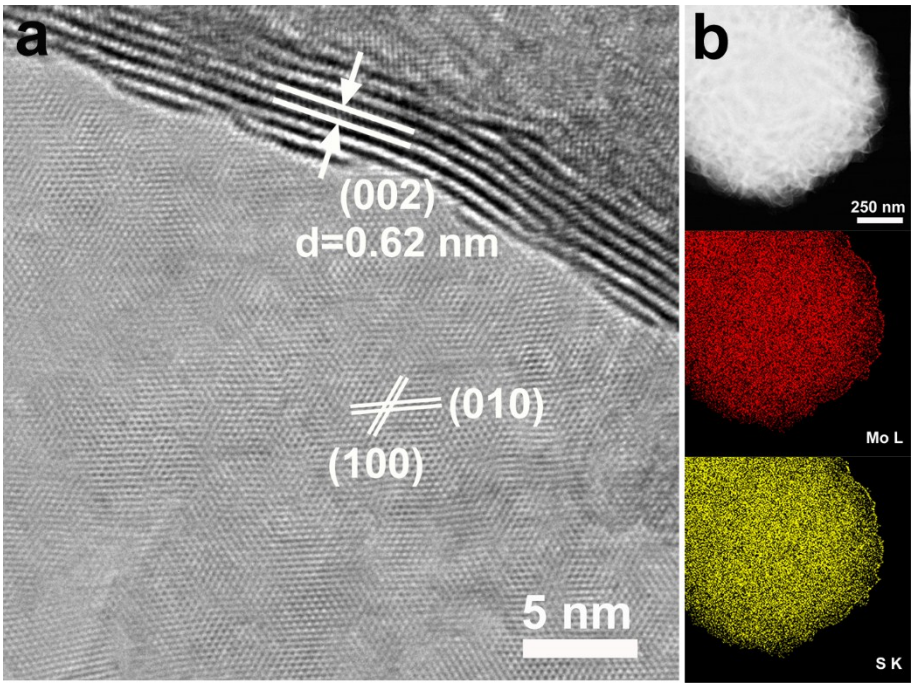

Figure S17. (a) HRTEM image of MoS_2. (b) Element mappings of Mo and S.

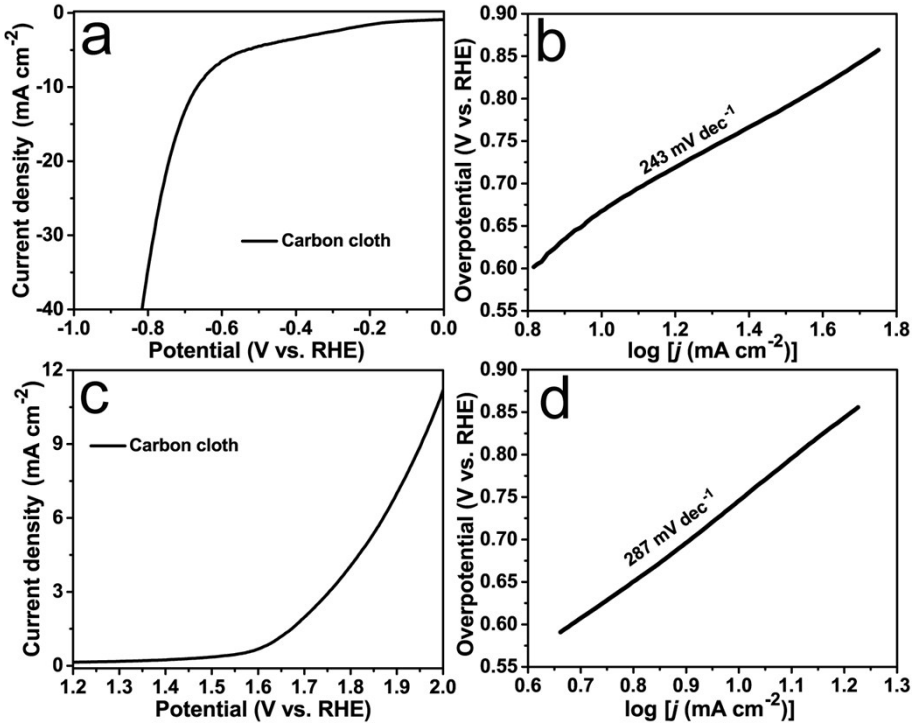

Figure S18. (a) LSV curve and (b) Tafel slope of pure carbon cloth (CC) for HER in 1 M KOH. (c) LSV curve and (d) Tafel slope of CC for OER in 1 M KOH.

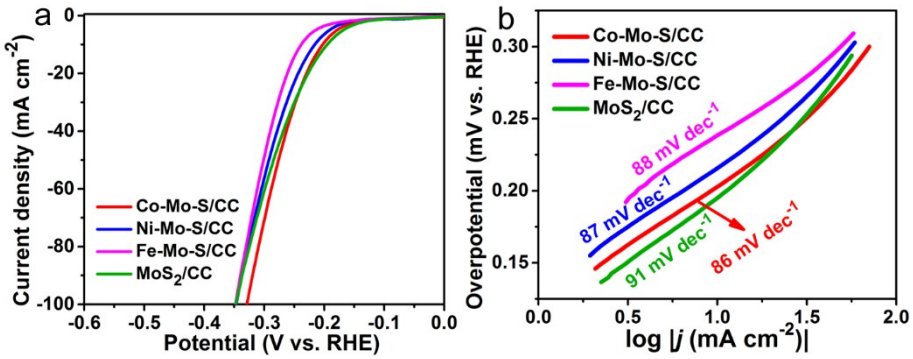

Figure S19. (a) LSV curve and (b) Tafel slope of Co-Mo-S/CC, Ni-Mo-S/CC, Fe-Mo-S/CC and MoS_2/CC measured in 0.5 M H_2SO_4.

According to the LSV curves measured in 0.5 M H_2SO_4, η_{10} of Co-Mo-S/CC, Ni-Mo-S/CC, Fe-Mo-S/CC and MoS_2/CC are 203, 215, 240 and 195 mV, respectively. And the corresponding Tafel slopes are 86, 87, 88 and 91 mV dec^{-1}. Therefore, the HER properties of M-Mo-S/CC and MoS_2/CC in acid electrolyte show little difference and are inferior to the corresponding performance in 1 M KOH.

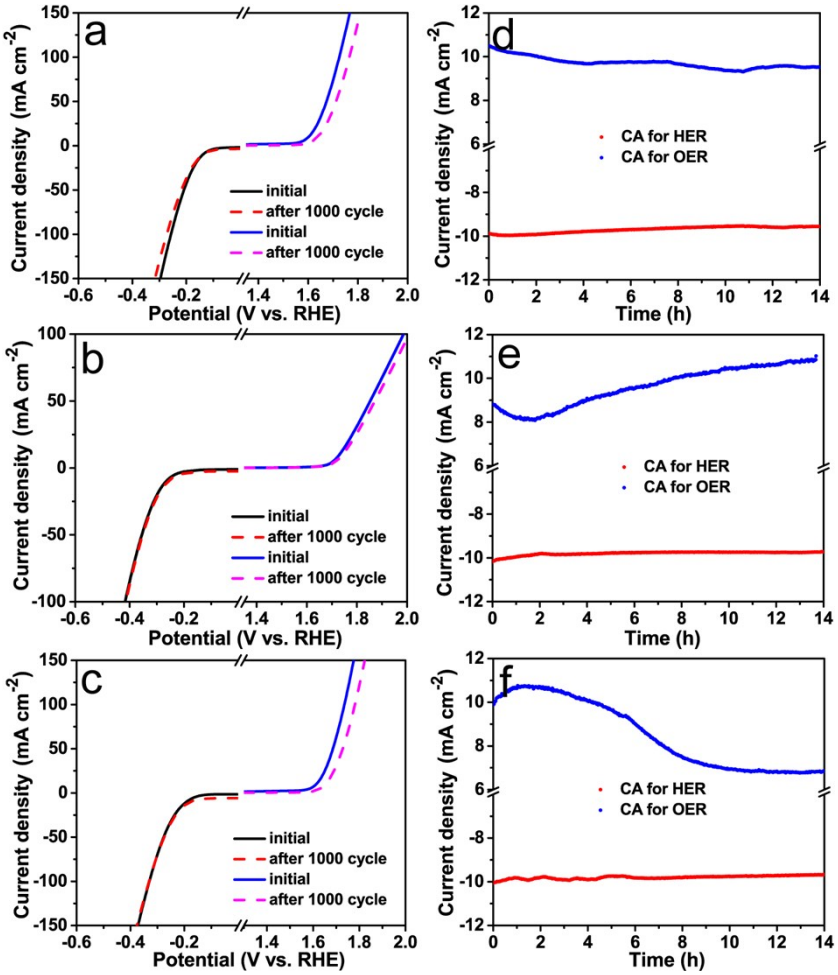

Figure S20. LSV curves of (a) Ni-Mo-S/CC, (b) Fe-Mo-S/CC, (c) MoS_2/CC before and after 1000 CV cycles for HER and OER in 1 M KOH. Chronoamperometric curves of (d) Ni-Mo-S/CC, (e) Fe-Mo-S/CC, (f) MoS_2/CC for HER and OER with a duration of 14 h in 1 M KOH.

According to CA curves of Co-Mo-S/CC, the current density retention is 100% for HER and 96% for OER. These results declare that Co-Mo-S/CC possesses excellent electrocatalytic stability, which is closely related to the unique morphology and heterostructure. Co-Mo-S particles have regular sizes and can be decorated on carbon fiber densely and uniformly. Besides, the unique heterostructure with CoS_2 mainly inside and MoS_2 nanosheets outside ensures the stability of Co-Mo-S particles. In contrast, the current density retention of Ni-Mo-S/CC is only 96.8% for HER and 90.5% for OER, suggesting the inferior stability than Co-Mo-S/CC. Ni-Mo-S/CC has large-sized (>1 μm) and irregular spherical particles, which are easy to peel off from CC substrates. Separately, CA curve of Fe-Mo-S/CC for OER shows 22.5% current increase owing to the primary activated process. MoS_2/CC shows poor CA stability, especially for OER measurement because of no transition metal doping. Moreover, MoS_2 particles with different size are grown on CC sparsely also leading to the inferior stability. Therefore, different morphologies and structures of M-Mo-S/CC have a great effect on their stability performance.

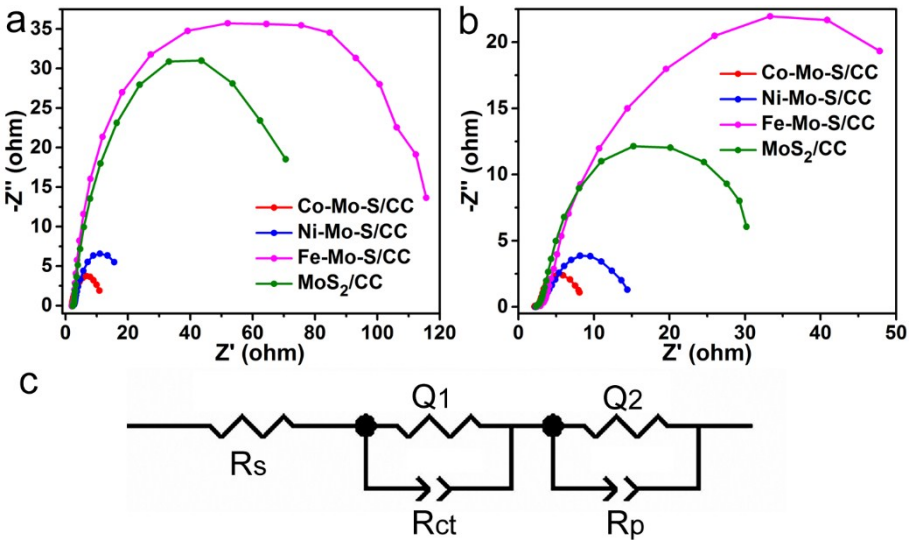

Figure S21. EIS spectrum of Co-Mo-S/CC, Ni-Mo-S/CC, Fe-Mo-S/CC and MoS_2/CC, (a) recorded at overpotential of 150 mV vs. RHE for HER in 1 M KOH and (b) recorded at overpotential of 300 mV vs. RHE for OER in 1 M KOH. (c) The equivalent electric circuit used for fitting analysis.

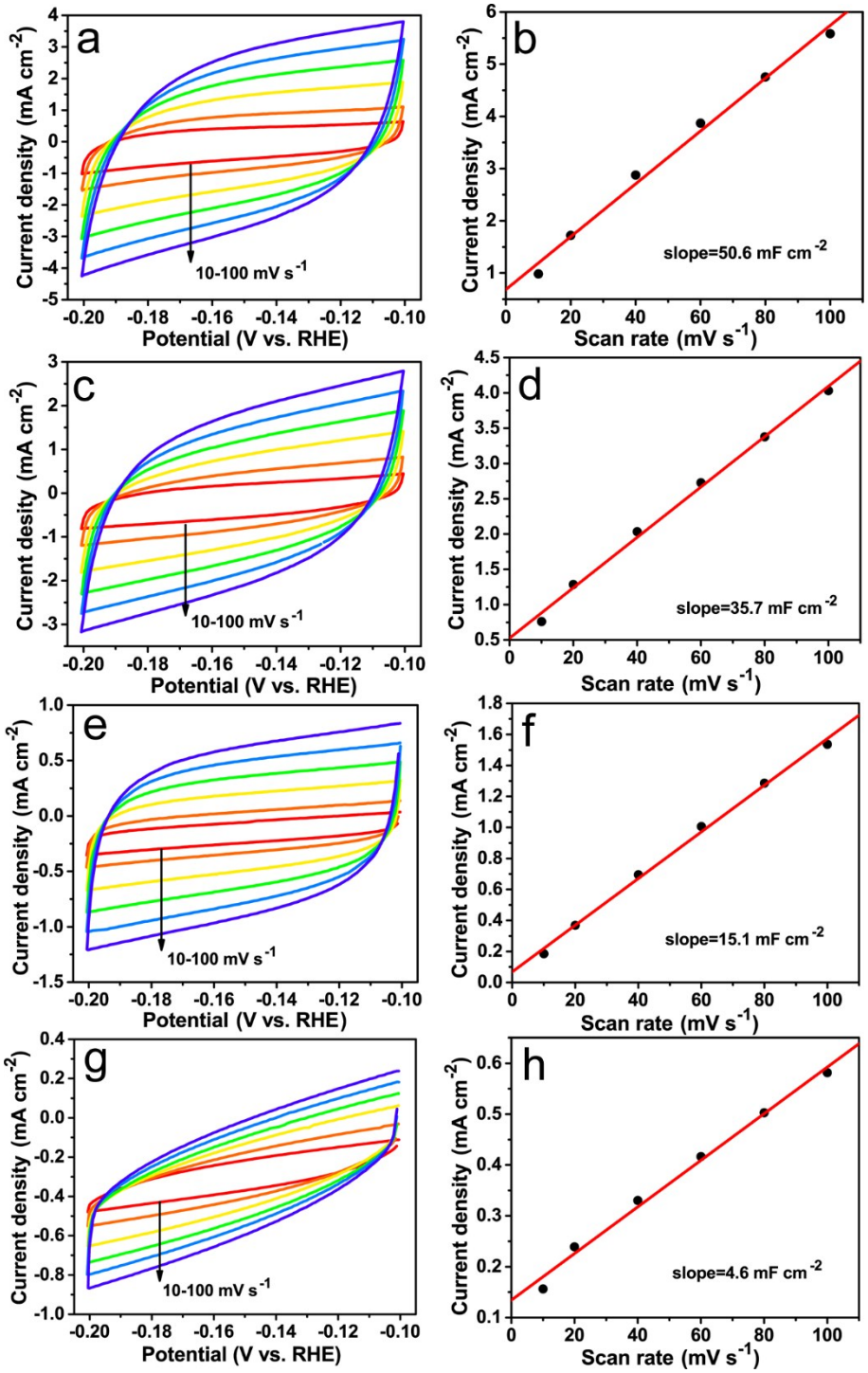

Figure S22. CV curves between the potential of -0.2 and -0.1 V vs. RHE at different scan rate (10-100 mV s^{-1}) in 1 M KOH for (a) Co-Mo-S/CC, (c) Ni-Mo-S/CC, (e) Fe-Mo-S/CC and (g) MoS_2/CC. Double-layer capacitance (C_{dl}) according to the CV curves for (b) Co-Mo-S/CC, (d) Ni-Mo-S/CC, (f) Fe-Mo-S/CC and (h) MoS_2/CC.

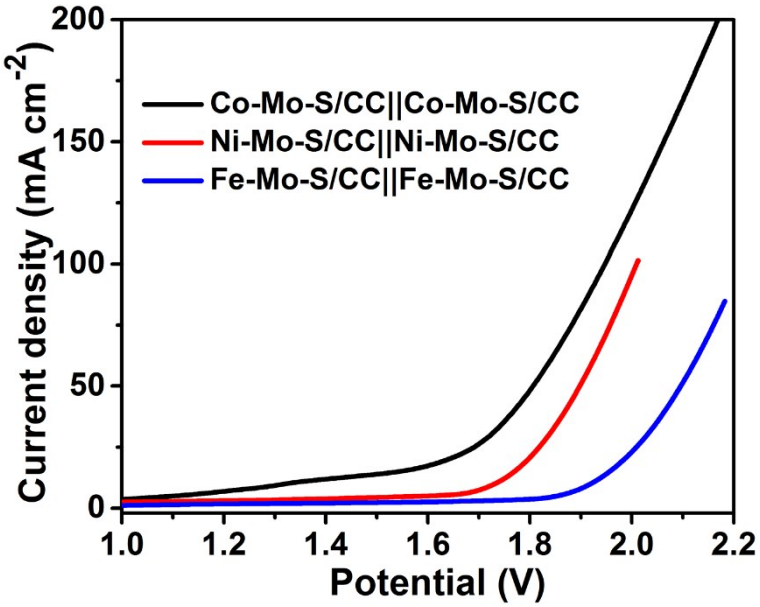

Figure 23. LSV curves of overall water splitting for Co-Mo-S/CC||Co-Mo-S/CC, Ni-Mo-S/CC||Ni-Mo-S/CC and Fe-Mo-S/CC||Fe-Mo-S/CC.

Table S1. Crystal data and structure refinement for POMs of $CoMo_6$.

	$CoMo_6$
Empirical formula	$CoH_{12}Mo_6N_4O_{30}$
Formula weight	1182.17
Crystal system	Monoclinic
Space group	$P2_1/c$
a (Å)	11.403(14)
b (Å)	10.995(13)
c (Å)	11.715(14)
α (°)	90.000
β (°)	100.143(17)
γ (°)	90.000
V (Å^3)	1446(3)
Z	2
D_{calc}(g·cm^{-3})	2.717
Abs.coeff.(mm^{-1})	3.191
F(000)	1118.0
Reflns collected	8790/3287
GOFon F^2	1.140
R_{int}	0.0558
R_1[a]	0.0768
wR_2(all data)[b]	0.1641

[a] $R_1=\Sigma||F_o|-|F_c||/\Sigma|F_o|$. [b] $wR_2=|\Sigma w(|F_o|^2-|F_c|^2)|/\Sigma|w(F_o^2)^2|^{1/2}$

Table S2. Comparison of HER activities of Co-Mo-S/CC in this work and recently reported sulfides and other non-noble materials in alkaline electrolyte.

Catalyst	Substrate	Electrolyte	Mass loading (mg cm^{-2})	η_{10} (mV vs. RHE)	Reference
Co-Mo-S/CC	Carbon cloth	1 M KOH	1	118	This work
Ni-MoS_2	CC	1 M KOH	0.89	98	1
Ni_3FeN-NPs	GCE[a]	1 M KOH	0.35	158	2
NiCoP/rGO	CFP[b]	1 M KOH	0.15	209	3
$CoMoS_x$	Glassy carbon disks or polycrystalline gold	0.1 M KOH	0.05	215 (5 mA cm^{-2})	4
CoP@BCN-1	GCE	1 M KOH	0.4	215	5
Ni_3S_2/NF	Ni foam	1 M KOH	1.6	223	6
$Co_{0.85}Se$@NC	GCE	1 M KOH	0.4	230	7
$NiMo_3S_4$	GCE	0.1 M KOH	~0.3	257	8
$Co_{0.85}Se_2$/NiFe-LDH/graphene	Graphite foil	1 M KOH	4.0	260	9
Co/Co_9S_8@SNGS	RDE[c]	0.1 M KOH	0.305	350 (20 mA cm^{-2})	10

Note: [a] GCE means glassy carbon electrode, [b] CFP means carbon fiber paper, [c] RDE means rotating disk electrode.

Table S3. Comparison of OER activities of Co-Mo-S/CC in this work and recently reported sulfides and other non-noble materials in alkaline electrolyte.

Catalyst	Substrate	Electrolyte	Mass loading (mg cm^{-2})	η_{10} (mV vs. RHE)	Reference
Co-Mo-S/CC	Carbon cloth	1 M KOH	1	300	This work
Ni_3S_2/NF	Ni foam	1 M KOH	1.6	260	6
$Ni_{2.3\%}$-CoS_2	Carbon cloth	1 M KOH	0.97	~300	11
$Co_{0.85}$Se@NC	GCE	1 M KOH	0.4	320	7
Zn-Co-S	CFP	1 M KOH	0.6	320	12
$Zn_{0.76}Co_{0.24}S/CoS_2$	Ti mesh	1 M KOH	1.0	330 (at 20 mA cm^{-2})	13
NiS	Ni foam	1 M KOH	43	335 (at 50 mA cm^{-2})	14
$NiCo_2S_4$ NA	Carbon cloth	1 M KOH	4.0	340 (at 100 mA cm^{-2})	15
N-Co_9S_8/G	GCE	0.1 M KOH	0.2	409	16
$Co_{0.5}Fe_{0.5}$S@N-MC	GCE	1 M KOH	0.8	410	17

Table S4. Comparison of current density retention (%) after 14 h CA measurements for corresponding samples in 1 M KOH.

	Co-Mo-S/CC	**Ni-Mo-S/CC**	**Fe-Mo-S/CC**	**MoS_2/CC**
HER	100%	96.8%	95.4%	98.3%
OER	96.0%	90.5%	122.3%	69.2%

Table S5. Comparison of R_{ct} values for corresponding samples recorded in 1 M KOH.

	Co-Mo-S/CC	**Ni-Mo-S/CC**	**Fe-Mo-S/CC**	**MoS_2/CC**
R_{ct} for HER	9.3 Ω	15.9 Ω	106 Ω	75.3 Ω
R_{ct} for OER	4.9 Ω	9.7 Ω	57.7 Ω	28.4 Ω

Table S6. Comparison of overall water splitting performance of Co-Mo-S/CC in this work and other recently reported representative electrocatalysts.

Elelctrocatalyst	Electrolyte	Substrate	Mass loading (mg cm^{-2})	Current Density (mA cm^{-2})	Potential (V)	Reference
Co-Mo-S/CC||Co-Mo-S/CC	1 M KOH	Carbon cloth	1	20	1.64	This work
				50	1.80	
Co/Co_9S_8@SNGS||Co/Co_9S_8@SNGS	0.1 M KOH	Ni foam	1	20	1.58	10
NiCoP/rGO||NiCoP/rGO	1 M KOH	CFP	0.15	10	1.59	3
Ni/NiP||Ni/NiP	1 M KOH	Ni foam	/	10	1.61	18
CoP-MNA||CoP-MNA	1 M KOH	Ni foam	6.2	10	1.62	19
				20	1.66	
Co_9S_8@NOSC-900||Co_9S_8@NOSC-900	1 M KOH	Ni foam	5	10	1.60	20
				20	1.74	
$CoNi(OH)_x$||NiN_x	1 M KOH	Cu foil	/	11	1.65	21
FeCo||FeCoNi-2	1 M KOH	Carbon paper	1	10	1.687	22
$Co_{0.85}$Se@NC||$Co_{0.85}$Se@NC	1 M KOH	Ni foam	/	10	1.76	7
Ni_3S_2/NF||Ni_3S_2/NF	1 M KOH	Ni foam	1.6	~13	~1.76	6

Notes and references

1 J. Zhang, T. Wang, P. Liu, S. Liu, R. Dong, X. Zhuang, M. Chen and X. Feng, *Energy Environ. Sci.*, 2016, **9**, 2789-2793.

2 X. Jia, Y. Zhao, G. Chen, L. Shang, R. Shi, X. Kang, G. I. N. Waterhouse, L.-Z. Wu, C.-H. Tung and T. Zhang, *Adv. Energy Mater.*, 2016, **6**, 1502585-1502590.

3 J. Li, M. Yan, X. Zhou, Z.-Q. Huang, Z. Xia, C.-R. Chang, Y. Ma and Y. Qu, *Adv. Funct. Mater.*, 2016, **26**, 6785-6796.

4 J. Staszak-Jirkovsky, C. D. Malliakas, P. P. Lopes, N. Danilovic, S. S. Kota, K.-C. Chang, B. Genorio, D. Strmcnik, V. R. Stamenkovic, M. G. Kanatzidis and N. M. Markovic, *Nat. Mater.*, 2016, **15**, 197-203.

5 H. Tabassum, W. Guo, W. Meng, A. Mahmood, R. Zhao, Q. Wang and R. Zou, *Adv. Energy Mater.*, 2017, **7**, 1601671-1601677.

6 L.-L. Feng, G. Yu, Y. Wu, G.-D. Li, H. Li, Y. Sun, T. Asefa, W. Chen and X. Zou, *J. Am. Chem. Soc.*, 2015, **137**, 14023-14026.

7 T. Meng, J. Qin, S. Wang, D. Zhao, B. Mao and M. Cao, *J. Mater. Chem. A*, 2017, **5**, 7001-7014.

8 J. Jiang, M. Gao, W. Sheng and Y. Yan, *Angew. Chem. Int. Ed.*, 2016, **128**, 15466-15471.

9 Y. Hou, M. R. Lohe, J. Zhang, S. Liu, X. Zhuang and X. Feng, *Energy Environ. Sci.*, 2016, **9**, 478-483.

10 X. Zhang, S. Liu, Y. Zang, R. Liu, G. Liu, G. Wang, Y. Zhang, H. Zhang and H. Zhao, *Nano Energy*, 2016, **30**, 93-102.
11. W. Fang, D. Liu, Q. Lu, X. Sun and A. M. Asiri, *Electrochem. Commun.*, 2016, **63**, 60-64.
12. X. Wu, X. Han, X. Ma, W. Zhang, Y. Deng, C. Zhong and W. Hu, *ACS Appl. Mater. Interfaces*, 2017, **9**, 12574-12583.
13. Y. Liang, Q. Liu, Y. Luo, X. Sun, Y. He and A. M. Asiri, *Electrochim. Acta*, 2016, **190**, 360-364.
14. W. Zhu, X. Yue, W. Zhang, S. Yu, Y. Zhang, J. Wang and J. Wang, *Chem. Commun.*, 2016, **52**, 1486-1489.
15. D. Liu, Q. Lu, Y. Luo, X. Sun and A. M. Asiri, *Nanoscale*, 2015, **7**, 15122-15126.
16. S. Dou, L. Tao, J. Huo, S. Wang and L. Dai, *Energy Environ. Sci.*, 2016, **9**, 1320-1326.
17. M. Shen, C. Ruan, Y. Chen, C. Jiang, K. Ai and L. Lu, *ACS Appl. Mater. Interfaces*, 2015, **7**, 1207-1218.
18. G.-F. Chen, T. Y. Ma, Z.-Q. Liu, N. Li, Y.-Z. Su, K. Davey and S.-Z. Qiao, *Adv. Funct. Mater.*, 2016, **26**, 3314-3323.
19 Y.-P. Zhu, Y.-P. Liu, T.-Z. Ren and Z.-Y. Yuan, *Adv. Funct. Mater.*, 2015, **25**, 7337-7347.
20 S. Huang, Y. Meng, S. He, A. Goswami, Q. Wu, J. Li, S. Tong, T. Asefa and M. Wu, *Adv. Funct. Mater.*, 2017, **27**, 1606585-1606594.
21 S. Li, Y. Wang, S. Peng, L. Zhang, A. M. Al-Enizi, H. Zhang, X. Sun and G. Zheng, *Adv. Energy Mater.*, 2016, **6**, 1501661-1501667.
22 Y. Yang, Z. Lin, S. Gao, J. Su, Z. Lun, G. Xia, J. Chen, R. Zhang and Q. Chen, *ACS Catal.*, 2017, **7**, 469-479.